The Kinetic Influence of Siliceous Reactions on Structure Formation of Mesoporous Silica Formed via the Co-Structure Directing Agent Route

Ruiyu Lin,[†] Göran Carlström,[‡] Quoc Dat Pham,[†] Michael W. Anderson,[||] Daniel Topgaard,[†] Karen J. Edler,[†,§] and Viveka Alfredsson[,†]*

[†] Division of Physical Chemistry, Lund University, SE-22100 Lund, Sweden

[‡] Centre for Analysis and Synthesis, Lund University, SE-22100 Lund, Sweden

[||] Centre for Nanoporous Materials, School of Chemistry, University of Manchester, Manchester, M13 9PL, U.K.

[§] Department of Chemistry, University of Bath, Bath, BA2 7AY, U.K.

Abstract

We investigate the mechanism responsible for the formation of mesoporous silica formed with the so-called co-structure directing agent (CSDA) route. The synthesis relies on the interaction between silica source (tetraethylorthosilicate), cationic surfactant ($C_{18}H_{37}N^{+}(CH_3)_2(CH_2)_3N^{+}(CH_3)_3Br_2$) and CSDA (carboxyethylsilanetriol), that results in a material functionalized with carboxylic groups. Depending on the concentration of HCl in the synthesis, the structure is defined by $Fm\bar{3}m$ (at high pH) and by $Fd\bar{3}m$ (at low pH), with a gradual transition in the intermediate pH range. Here we aim at finding the origin for the structural change triggered by pH and investigate the effects of the hydrolysis of the silica source on the overall kinetics of the synthesis. A fast process results in $Fm\bar{3}m$, regardless of pH, and a slow process results in $Fd\bar{3}m$. The hydrolysis step is the important structural control parameter. We studied the cross-linking of silica and CSDA using ^{29}Si NMR. The cross-linking is similar for the two structures, and possibly $Fd\bar{3}m$ structure contains slightly more CSDA. ^{13}C PT ssNMR was used to investigate the surfactant mobility/rigidity during the synthesis. The rigidity of the $Fm\bar{3}m$ is established much faster than the $Fd\bar{3}m$.

1. Introduction

Mesoporous silica materials are produced in a self-assembly process between amphiphilic molecules and an inorganic silica source in an aqueous solution.[1] Removal of the organic matter after completed synthesis establishes the porous network.[1] In the earliest work, cationic surfactants were employed as structure directing agents.[2-3] This strategy was soon followed by the use of other efficient structure directors, such as amphiphilic block-copolymers, Pluronics.[4-5] With these systems it was clear that amphiphiles with either cationic or non-ionic headgroups could interact with siliceous species resulting in the formation of ordered mesoporous silica materials, whereas anionic surfactants were unable to function in a similar way. However in 2003, with the advent of a new synthesis methodology making use of a so-called co-structure directing agent (CSDA), Che and co-workers demonstrated that anionic surfactants could also function as versatile structure promoters.[6] It was clear that the CSDA route permitted the formation of several structures that had not previously been synthesized, such as the bicontinuous cubic structure $Pn\bar{3}m$ [7] and chiral materials [8]. It was subsequently found that also cationic surfactants can be employed in the CSDA approach.[9] The CSDA is an organosilane molecule, which contains a charged group, typically from an acid, or a base, and a silicate group.[7] It is suggested that the CSDA forms a "bridge" between the charged head group of the surfactant and the silica wall. If the synthesis is based on cationic surfactants, the CSDA has a negatively charged group and for synthesis with anionic surfactants it is positively charged.[7]

In a typical synthesis using the CSDA method, different structures can be formed within one synthesis system by simply controlling the pH.[7, 9] For instance, in 2007, Han et al. synthesized, in a one-pot synthesis, mesoporous silicas functionalized with carboxylic groups using this approach.[10] The cationic surfactant octadecylpentamethyl-1,3-propylenebis(ammonium

bromide), $C_{18}H_{37}N^{+}(CH_3)_2(CH_2)_3N^{+}(CH_3)_3Br_2$ (designated as $C_{18\text{-}3\text{-}1}$), was used as the template and carboxyethylsilanetriol sodium salt, $Si(OH)_3(CH_2)_2COONa$, was used as the CSDA. It was observed that, with increasing concentration of HCl, a mesostructure transformation took place. Low concenration of HCl resulted in a material consisting of a mixture of cubic close packing CCP (*i.e*. $Fm\bar{3}m$) and hexagonal close packing HCP (*i.e.* $P6_3/mmc$) of entities based on spherical micelles. High concentration of HCl resulted in the $Fd\bar{3}m$ structure. Intermediate concentration of HCl resulted in a gradual transformation from the $Fm\bar{3}m$ (mixed with $P6_3/mmc$) to the $Fd\bar{3}m$ structure as the HCl concentration increased.[11] The structural extremes as well as the structural transformation have been analysed in detail with high-resolution transmission electron microscopy.[11] The close-packed structures consist of, as already mentioned, spheres, whereas the $Fd\bar{3}m$ structure is composed of polyhedra.[11-12] The polyhedra have been explained to arise from packing of "soft-cages" [13], *i.e.* the softness of the micellar entity allows it to form an interface to its neighbor thereby creating a polyhedron.[11]

Some effort has, for about two decades, been invested in studying the formation mechanism of mesoporous silica material, particularly the MCM-41 and SBA-15 systems.[14-15] However, less is known about the synthesis via the CSDA approach.[16] We are interested in shedding more light onto the mechanism of the formation process used in the CSDA approach, and, in this study, we focus on the synthesis system described above (using $C_{18\text{-}3\text{-}1}$ and carboxyethylsilanetriol sodium salt) and aim at finding the origin for the structural change triggered by pH.

The structural transformation has been suggested to occur as a consequence of the ionization degree of the CSDA.[10, 13] The CSDA contains a carboxylic group, which typically has a *pKa* in the range of 1-5. The difference in pH was therefore suggested to influence the strength of the electrostatic interaction between the surfactant head group and the carboxylic group of the

CSDA, as a consequence of the varying ionization degree of the CSDA. However, in this pH range the rate of the TEOS reactions (*i.e.* the hydrolysis and subsequent silica polymerization) varies to a great extent. The hydrolysis rate of TEOS reaches a minimum at a pH around 7. The condensation on the other hand shows a reverse behavior with the highest rate just around pH 8.[17-18]

We noticed that at pH around 7, where the hydrolysis rate of TEOS is low, the $Fd\bar{3}m$ structure is formed. Hence, a complicating aspect in this system is the variation of the kinetics of the reactions. In this work, we have investigated the effects of the kinetics of the hydrolysis on the structural transformation between the $Fm\bar{3}m$ (intergrown with $P6_3/mmc$) structure and the $Fd\bar{3}m$ structure. Henceforth we will use the notation $Fm\bar{3}m$ for the structure dominated by this space group even though it is to some extent intergrown with $P6_3/mmc$. We have used two simple methods both related to the kinetics of hydrolysis. In one set of experiments we removed the influence of TEOS hydrolysis by hydrolysing the TEOS prior to addition to the synthesis. In another set we slowed down the hydrolysis reaction by adding ethanol, hence shifting the equilibrium reaction in accordance with le Châtelier's principle.

We have also used solid-state ^{29}Si NMR to investigate the extent of crosslinking of silica and CSDA, respectively, for the materials obtained with and without pre-hydrolysis of TEOS. Both cubic structures ($Fm\bar{3}m$ & $Fd\bar{3}m$) were thus investigated.

In an effort to investigate the mobility of the surfactants at the early stage of the synthesis, we have used ^{13}C Polarization Transfer solid-state NMR (^{13}C PT ssNMR)[19-20]. PT ssNMR consists of three separate experiments, direct polarization (DP), cross polarization (CP),[21] and refocused insensitive nuclei enhanced by polarization transfer (INEPT).[22-25] The DP spectra give semi-quantitative information about the ^{13}C present in the sample, while the CP and the INEPT spectra

indicate the mobility of the C-H bonds in the molecules. A high CP signal is obtained with a rigid ^{13}C and a high INEPT signal is attained from a mobile or isotropic ^{13}C. Combination of these three experiments provides segmental resolution (*i.e.* ^{13}C in CH, CH_2, CH_3) due to the different chemical shifts, and qualitative information on the molecular dynamics of each resolved ^{13}C segment. The PT ssNMR method has previously been used to get qualitative information on molecular dynamics with atomic resolution of surfactants [19-20] and lipids [26]. Here we show that PT ssNMR is a valuable technique for getting mobility information of the surfactants during the formation process of mesostructured inorganic materials.

In this paper, we first discuss how the kinetics of TEOS hydrolysis controls the structure by showing results from syntheses where the kinetics have been altered. Secondly, we discuss the extent of cross-linking of silica and CSDA in the structures based on ^{29}Si NMR analysis. Finally, we explore PT ssNMR results regarding the surfactant mobility/rigidity in the two structures as a function of synthesis time.

2. Experimental Section

2.1. Chemicals

The silica source, tetraethyl orthosilicate (TEOS, from SCRC, Germany) and the CSDA, carboxyethylsilanetriol sodium salt (from ABCR, Germany), were used as received without further purification. The surfactant $[C_{18}H_{37}N(CH_3)_2(CH_2)_3N(CH_3)_3]Br_2$ ($C_{18\text{-}3\text{-}1}$) was kindly provided by Prof. Shunai Che in Shanghai Jiao Tong University, China. It was synthesized according to a previously reported procedure,[10] and used as received.

2.2. Synthesis of the mesoporous materials

The materials were synthesized under various concentrations of HCl and in some cases with addition of ethanol. A normal synthesis was performed as follows: 1.40 g of $C_{18\text{-}3\text{-}1}$ was dissolved in 9.00 g of MilliQ water in a 30 mL fluorinated ethylene propylene (FEP) bottle, and HCl (from 1M stock solution) and ethanol (99.7 volume%), with different molar composition of HCl (x) and of ethanol (y). To this solution 0.348 g of CSDA and 0.78 g of TEOS were added simultaneously. The final composition was $C_{18\text{-}3\text{-}1}$: CSDA: TEOS: HCl: ethanol: H_2O = 1: 2: 15: x : y : 2000 ($x = 0 \sim 2.4, y = 0 \sim 120$). For the pre-hydrolysis experiment, TEOS was hydrolyzed in 1 mL 0.07 M HCl solution for 5 min before this solution was added to the synthesis solution together with the CSDA. The rest of the synthesis solution (amount of HCl and H_2O) was changed accordingly to keep the ultimate composition the same as in the normal synthesis.

The mixture was stirred for 2 h at room temperature and then hydrothermally treated at 100 ^oC under static conditions for 2 days. pH measurements were performed after 2 days of hydrothermal treatment. The resulting white precipitates were collected by filtration, washed with distilled water, and dried at room temperature. For the purpose of nitrogen sorption experiments, the surfactant was removed from the as-made material by calcination at 550 ^oC for 6 h. In order to retain the carboxylic groups, i.e. to maintain a functional material, the surfactants should be removed by extraction [10].

2.3. Small Angle X-ray Diffraction (SAXD)

The SAXD patterns were recorded using a Ganesha 300XL SAXSLab instrument from JJ-Xray Systems, equipped with a sealed micro-focus X-ray tube (Rigaku) and a 2D 300 K Pilatus

detector (Dectris). Measurements were performed using a pin-hole collimated beam with an asymmetrically positioned detector yielding a single measurement q-range of 0.0012–0.67 $Å^{-1}$. The scattering vector is defined as $q = 4\pi/\lambda \sin\theta$, where λ is the incoming X-ray wavelength, 1.54 Å, and θ is half of the scattering angle. The samples were contained in 2 mm (diameter) quartz glass capillaries with 0.01 mm thickness (Hilgenberg), and each measurement was performed for 10 min.

2.4. Solid-state NMR

^{29}Si NMR spectra were collected on a Bruker MSL 400 solid-state NMR spectrometer using double-bearing magic-angle spinning (MAS) zirconia rotors with high-power proton decoupling at 79.48 MHz using a 90° pulse with a 2 min repetition time (450 scans). All ^{29}Si spectra were recorded on samples spun at 5922 Hz in a 4 mm rotor and referenced to TMS.

^{13}C NMR spectra were recorded on a Bruker Avance-II 500 spectrometer with an 11.7 T magnetic field and a 4 mm CP/MAS HCP Efree probe. ^{1}H and ^{13}C resonance frequencies were 500 and 126 MHz, respectively. The MAS frequency was 5 kHz. Samples were packed in 4 mm rotors (Bruker). The PT ssNMR (Polarization Transfer solid-state NMR)[19] experiments were carried out on the samples using a spectral width of 248 ppm, acquisition time of 50 ms, 1024 scans per experiment and 4 s recycle delay. The signal was acquired under 68 kHz TPPM-15 (Two Phase Pulse Modulated)[27] ^{1}H decoupling. Solid α-glycine (43.7 ppm) was used as external reference. ^{1}H and ^{13}C hard pulses were applied at nutation frequencies ${\omega_1}^{H/C}/2\pi = 80.6$ kHz. The CP (Cross Polarization)[21] experiment was performed with CP contact time $\tau_{CP} = 1$ ms, ${\omega_1}^{C}/2\pi = 72.6$ kHz and ${\omega_1}^{H}/2\pi$ linearly ramped from 64.5 to 80.6 kHz. The INEPT [23, 25]

experiment was optimized for a scalar coupling constant J_{CH} = 140 Hz (τ_1 = 1.79 ms), and a refocusing delay of $1/6J_{CH}$ giving positive peaks for all CH_x groups (τ_2 = 1.2 ms).

The data obtained were treated in ACD/NMR Processor Academic Edition (http://www.acdlabs.com/resources/freeware/nmr_proc/). A Lorentzian lineshape was used to fit the ^{29}Si data. The width is fitted between 25 to 1100 ppm.

2.5. N_2-sorption

The surface area, pore dimensions, and pore volumes were determined by nitrogen physisorption measurements at 77 K (ASAP 2010, Micromeritics Co., Norcross, GA). The specific surface area was deduced using the BET method at P/P_0 ratios between 0.05 and 0.2. The total pore volume was taken at $P/P_0 = 0.79$ hence removing the effect of macropores, which is significant for the materials synthesized with pre-hydrolysis step, in the analyses. The pore size was determined by DFT analysis (Micromeritics Co., Norcross, GA).

3. Results and discussion

3.1. Kinetics of TEOS hydrolysis

We reproduced the synthesis of Han *et al* [10], with x (HCl content) ranging from 0 to 2.4. The pH of the reaction solution was measured after the hydrothermal treatment. The resulting SAXD patterns (from as-synthesised materials) are shown in Figure S1 in the supporting information along with the corresponding pH values. The $Fm\bar{3}m$ structure was obtained in the pH range 8.5-11.0, the $Fd\bar{3}m$ structure in the range 5.0-7.5 and the material produced in the intermediate range (7.5-8.5) gave, as expected, SAXD pattern consistent with the intergrown phase. It is well known

that alkoxysilane reactions, both hydrolysis and subsequent condensation, are highly pH dependent [17] and the rates of both hydrolysis and condensation vary dramatically in the 5 - 11 pH interval covered in these synthesis. The $Fd\bar{3}m$ structure is obtained in the pH range where the hydrolysis rate has a minimum, whereas the $Fm\bar{3}m$ structure is obtained when this rate is higher. In order to investigate whether the hydrolysis rate has an effect on the structure, we performed two sets of experiment. This was done by either: i) introducing a pre-hydrolysis step in the synthesis, thereby removing the influence of TEOS hydrolysis [28], or ii) adding ethanol to the synthesis to slow down the hydrolysis - increasing the effect of this step.

i) Synthesis with pre-hydrolyzed TEOS

Figure 1 shows the SAXD patterns of materials obtained from a synthesis at three different pH values (Fig. 1A), producing the $Fm\bar{3}m$ (curve a), the $Fd\bar{3}m$ (curve c) or an intergrowth of these structures (curve b); it also shows the corresponding materials (Fig. 1B) obtained when TEOS was hydrolyzed for 5 minutes in 1 mL of 0.07 mol/L HCl solution prior to addition to the surfactant solution. The same total compositions are used in each corresponding set of experiments. It is clear that materials formed when TEOS was pre-hydrolyzed show similar SAXD pattern regardless of the pH of the solution. The formation under these conditions is thus pH independent. The peaks are less well defined compared with the materials in Figure 1A, but consistent with the $Fm\bar{3}m$ structure (the 111, 220 and 311 peaks are indexed in Figure 1B). The lattice spacings are in all three cases smaller than the $Fm\bar{3}m$ structure in Figure 1A, (see Table 1).

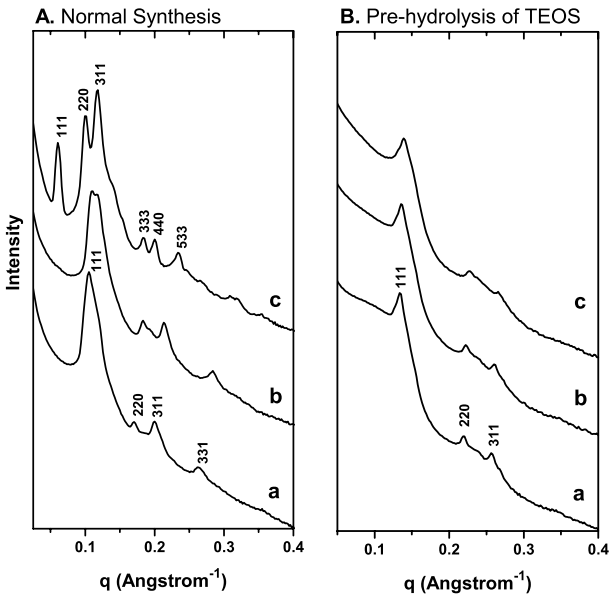

Figure 1. SAXD patterns of as-synthesized carboxylic group functionalized mesoporous silica materials, synthesised at different pH, a) pH=9, b) pH=8, c) pH=6, and using, A) normal synthesis, and B) with pre-hydrolysis of TEOS. The chemical molar composition of the reaction mixture was $C_{18\text{-}3\text{-}1}$: 2CSDA: xHCl: 15TEOS: 2000H_2O, a) x=1.4, b) x=1.6, c) x=1.8. The SAXD patterns are indexed with the $Fm\bar{3}m$ space group (1A-a, and 1B-a) and the $Fd\bar{3}m$ space group (1A-c)

Table 1. Structure and porous properties of the samples shown in Figure 1

Synthesis method	Synthesis pH	Structure	Lattice spacing a (nm)		S_{BET} (m^2g^{-1})	Pore Volume (cm^3g^{-1})	Pore Diameter (nm)
			As-synthesized	Calcined			
Normal Synthesis	9	$Fm\bar{3}m$	10.35	10.26	666	0.66	3.11
	6	$Fd\bar{3}m$	17.68	16.97	633	0.56	3.11
Pre-hydrolysis of TEOS	9	$Fm\bar{3}m$	8.13	8.04	779	0.75	3.09
	6	$Fm\bar{3}m$	7.85	7.69	778	0.69	3.07

The hydrolysis step of TEOS is made in a highly acidic solution, at a pH close to 1, where TEOS hydrolysis is a fast process and condensation is expected to be slow. ^{29}Si NMR measurement (Figure S2 in Supporting Information) on the pre-hydrolysis solution (measurement performed after 5 min hydrolysis) showed peaks in three shift regimes, at -72, around -81 and around -90 ppm. The first peak is consistent with a monomer (Q^0) of fully hydrolysed TEOS, and the other peaks are consistent with oligomeric species having Q^1 or Q^2 silicas [29]. Hence, the TEOS is fully hydrolyzed when added to the reaction solution and has, to some extent, condensed, possibly into small oligomers. In these syntheses the effect of the hydrolysis reaction has thus been removed. With oligomers present, the reacting silica components have reduced flexibility compared to monomers, which could explain why the resulting Bragg peaks are less well defined. We conclude that a fast process, obtained when the rate of hydrolysis is high, or when TEOS has been pre-hydrolysed, leads to the $Fm\bar{3}m$ structure regardless of the pH of the reaction solution.

The calcined materials were also investigated by N_2-sorption (the isotherms are shown in Figure S3 in supporting information), and the results, along with the lattice spacing calculated from the SAXD data of as-synthesised and calcined materials, are compiled in Table 1. For materials obtained in the normal synthesis, the $Fd\bar{3}m$ structure and the $Fm\bar{3}m$ structure have similar pore diameters. Compared to the normal $Fm\bar{3}m$ synthesis, the synthesis with the pre-hydrolysis step produced the $Fm\bar{3}m$ structure with smaller lattice spacing but almost the same pore diameter, although with a larger pore size variation, possibly due to the reduced flexibility of the silica. These results indicate that the materials synthesized with the pre-hydrolysis step are composed of thinner silica walls as compared to the normal material, which could also explain

the observation that the peaks are less intense. In addition, higher surface area and slightly higher pore volume were obtained for the pre-hydrolysed synthesis.

ii) Influence of addition of ethanol

Ethanol was added to the synthesis with the aim of slowing down the overall kinetics by shifting the equilibrium (equation 1) of the hydrolysis.

$$\equiv \mathrm{Si} - \mathrm{OCH_2CH_3} + \mathrm{H_2O} \leftrightarrow \equiv \mathrm{Si} - \mathrm{OH} + \mathrm{CH_3CH_2OH} \quad (1)$$

To the same three syntheses ($Fm\bar{3}m$, $Fd\bar{3}m$ and the intergrowth structures), different amounts of ethanol was added prior to the onset of the syntheses with the following molar ratios, EtOH:TEOS = 1:1, 2:1, 4:1, 8:1. The addition does not affect the pH in a significant way and the extent of dilution is small (10% of the solvent volume for the maximum addition). We observed that the precipitation was delayed and that the extent of the delay corresponded to the added amount of ethanol. Addition made to the intermediate pH range synthesis, *i.e.* at a pH of 8, resulted in a gradual structural change with increasing ethanol content (Fig. 2). Addition of ethanol, obtaining a EtOH:TEOS molar ratio of 2:1 (corresponding to curve c) and 4:1 (corresponding to curve d), facilitates the formation of the $Fd\bar{3}m$ structure. The peaks in curve c in Figure 2 are indexed with the $Fd\bar{3}m$ structure. The largest amount of ethanol (EtOH:TEOS molar ratio 8:1) results in a material where the structure is less well defined (Fig. 2 curve e). The synthesis mixtures typically resulting in the $Fm\bar{3}m$ (pH=9) and $Fd\bar{3}m$ structures (pH=6), respectively, were structurally unaffected by ethanol addition except for the largest addition (EtOH:TEOS=8:1) where no well ordered structure was obtained (see Figure S4 in supporting information).

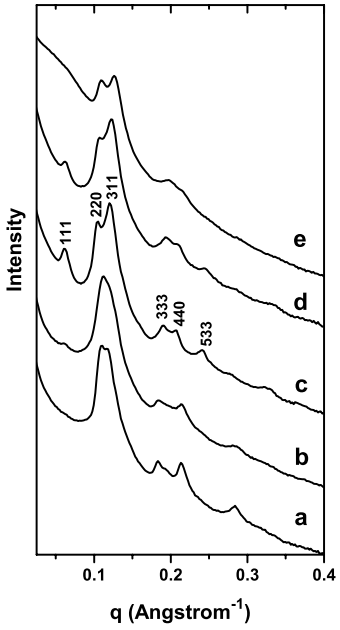

Figure 2. SAXD patterns of as-synthesized materials synthesized with addition of ethanol. The chemical molar composition of the reaction mixture was $C_{18\text{-}3\text{-}1}$: 2CSDA: 1.6HCl: 15TEOS: 2000H_2O: x EtOH, a) EtOH:TEOS=0 (x=0), b) EtOH:TEOS=1:1 (x=15), c) EtOH:TEOS=2:1 (x=30), d) EtOH:TEOS=4:1 (x=60), e) EtOH:TEOS=8:1 (x=120). Curve c is indexed with the $Fd\bar{3}m$ structure.

We conclude that addition of EtOH manages to "push" the formation towards the $Fd\bar{3}m$ structure if the structure is already present to some extent (as in the intergrowth structure), but is not "strong enough" to drive the formation all the way from the pure $Fm\bar{3}m$ structure. As we concluded with the pre-hydrolysis experiments above, the hydrolysis rate is a critical factor in determining which structure that results from the normal synthesis and that a slower process (produced with addition of EtOH) promotes the $Fd\bar{3}m$ structure.

3.2. Analysis of the cross-linking of silica and CSDA

It is clear that the kinetics of TEOS hydrolysis dictates the type of structure that forms, and in order to see if this is also reflected in the extent of cross-linking of silica, we used solid-state ^{29}Si NMR on as-synthesised materials. We investigated two synthesis conditions producing the $Fm\bar{3}m$ structure, at pH 9, and the $Fd\bar{3}m$ structures, at pH 6 (see Figure 1A, curves a and c), as well as the corresponding conditions with the pre-hydrolysis step, *i.e.* producing in both cases the $Fm\bar{3}m$ structure (See Figure 1B curves a and c). The resulting ^{29}Si NMR spectra are shown in Figure 3. The silicon environment Q^4 appears around -110 ppm, the Q^3 around -100 ppm, and Q^2 around -90 ppm.[30] It was also possible to determine the silica cross-linking of the CSDA. We use the notation T^3, T^2 and T^1 to represent the cross-linking environment of CSDA: T^3 appears around -66 ppm, T^2 around -57 ppm, and T^1 around -47 ppm.[29, 31] All four syntheses give rise to clear Q^3, Q^4, and T^3 signals, the T^2 is less clear but still identifiable. Q^1 and Q^2 are not discerned, except for the $Fd\bar{3}m$ structure (Fig. 3A-b) where the Q^1 is apparent. Peaks were fitted and integrated as described in the experimental section and the resulting values are shown in Table 2. The error with regard to the baseline is $\pm 10\%$ (estimated from the noise level variation to the average intensity of the peaks). The Q^1 and Q^2 peaks had too low intensity to be quantified so the extent of crosslinking is based on the ratio of the other peaks. Overall, based on Q^3/Q^4, the extent of condensation of the two structures is comparable. The $Fd\bar{3}m$ structure, in addition, contains a fraction of Q^1 species. In Table 2, $Q_{(sum)}$ is the sum of all Q peaks, and $T_{(sum)}$ is the sum of all T peaks, hence $Q_{(sum)}$ represents the entire amount of silica originating from TEOS, and $T_{(sum)}$ is the amount originating from CSDA. In the $Fm\bar{3}m$ structure, the ratio of $T_{(sum)}/Q_{(sum)}$ is 0.11, while for the $Fd\bar{3}m$ structure, this ratio is slightly larger, i.e. 0.13. This suggests that formation of the $Fd\bar{3}m$ structure requires more CSDA than does the $Fm\bar{3}m$ structure. The molar ratio of CSDA to

TEOS in the synthesis mixture is 0.13, demonstrating that both structures require a large uptake of CSDA. The T^2 to T^3 ratio in the $Fd\bar{3}m$ structure is higher than in the $Fm\bar{3}m$ structure, suggesting that the CSDA in the $Fd\bar{3}m$ structure is less cross-linked.

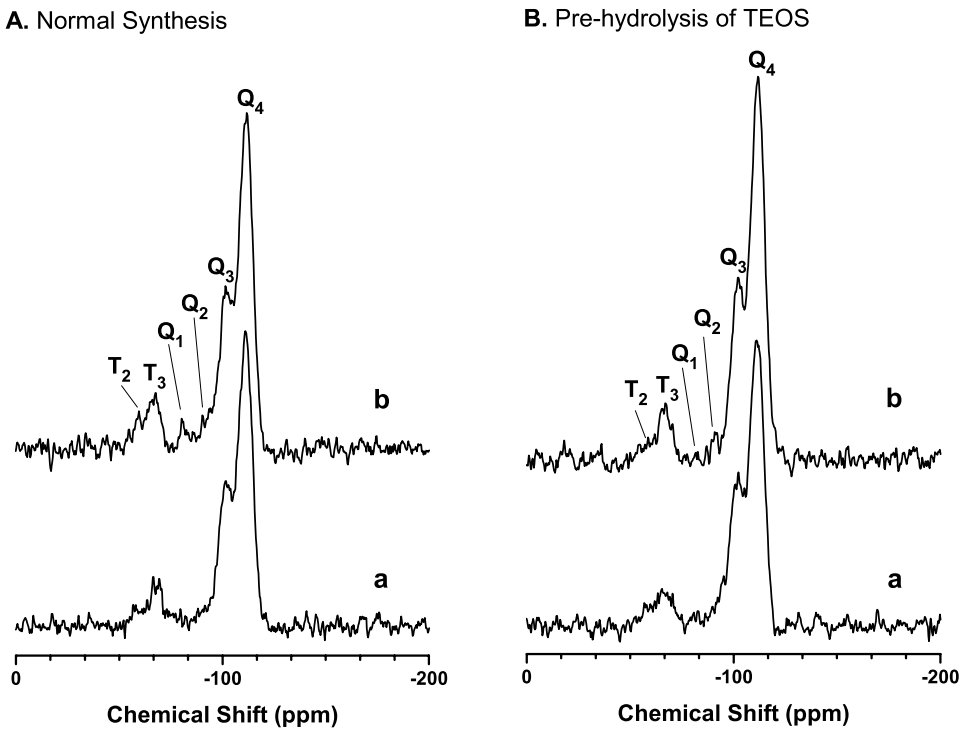

Figure 3. Solid-state ^{29}Si NMR spectra of samples shown in Figure 1. a) pH=9, b) pH=6, and, A) normal synthesis, B) pre-hydrolysis of TEOS. The chemical molar composition of the reaction mixture was $C_{18\text{-}3\text{-}1}$: 2CSDA: xHCl: 15TEOS: $2000H_2O$, a) x=1.4, b) x=1.8. The fits of the peaks are shown in the supporting information, Figure S5.

Table 2. Silica cross-linking values based on solid-state ^{29}Si NMR results. Q refers to the silica and q to the CSDA

Synthesis method	Synthesis pH	Structure	Q^4	Q^3	T^3	T^2	Q^3/Q^4	T^2/T^3	$T_{(sum)}/Q_{(sum)}$
Normal Synthesis	9	$Fm\bar{3}m$	0.53	0.36	0.08	0.02	0.68	0.25	0.11
	6	$Fd\bar{3}m$	0.50	0.33	0.07	0.04	0.66	0.57	0.13
Pre-hydrolysis of TEOS	9	$Fm\bar{3}m$	0.52	0.39	0.08	0.02	0.75	0.25	0.11
	6	$Fm\bar{3}m$	0.61	0.29	0.08	0.02	0.48	0.25	0.11

3.3. Behavior of the surfactants at the early stage of the synthesis

In an effort to investigate the mobility/rigidity of the surfactants we used ^{13}C PT ssNMR measurements. As previously mentioned, the CP and INEPT signals provide information about the rigidity and mobility coupled with the isotropic and anisotropic C-H bond reorientation. Information for each segment of the molecules can be explored. For comparison we investigated the liquid crystals formed in the pure water-surfactant ($C_{18\text{-}3\text{-}1}$) system. Two types of micellar cubic structures are stable [32]: one at 45 weight% water, and the other at 55 weight% water (Supporting Information, Figure S6). Both of these structures give rise to similar DP, CP and INEPT signals, with high (red) INEPT signals and very low (blue) CP signals, indicating that all the segments are predominantly mobile (Supporting Information, Figure S6). For the silica materials, the PT ssNMR measurements were performed on the as-synthesized samples at different synthesis stages: after 2 hours of reaction and after 2 days of hydrothermal treatment. In addition, as the mobility of the surfactants in the $Fd\bar{3}m$ structure was significantly different at these points in time, this structure was also investigated in the interim window, after 1.5 and 7 hours of hydrothermal treatment, respectively.

In Figure 4 the chemical structures of the surfactant and the CSDA are depicted with respect to the different mobility of the carbon segments, illustrated as circles. The segments are numbered with Arabic numbers (1-26) in the surfactant molecule and with Roman numbers in the CSDA (I-III). In addition the methylene and methyl groups, in ethanol or TEOS, are numbered IV and V respectively. The following colors are used to illustrate the signals: red - INEPT, blue - CP and grey - DP. For segments that show both INEPT and CP intensities, purple circles are used. When several peaks overlap, like the 22, II, and V, the accurate mobility cannot be determined; these segments are represented by black circles. Hence segment 22 and II could not be analyzed and are not included in the discussion below.

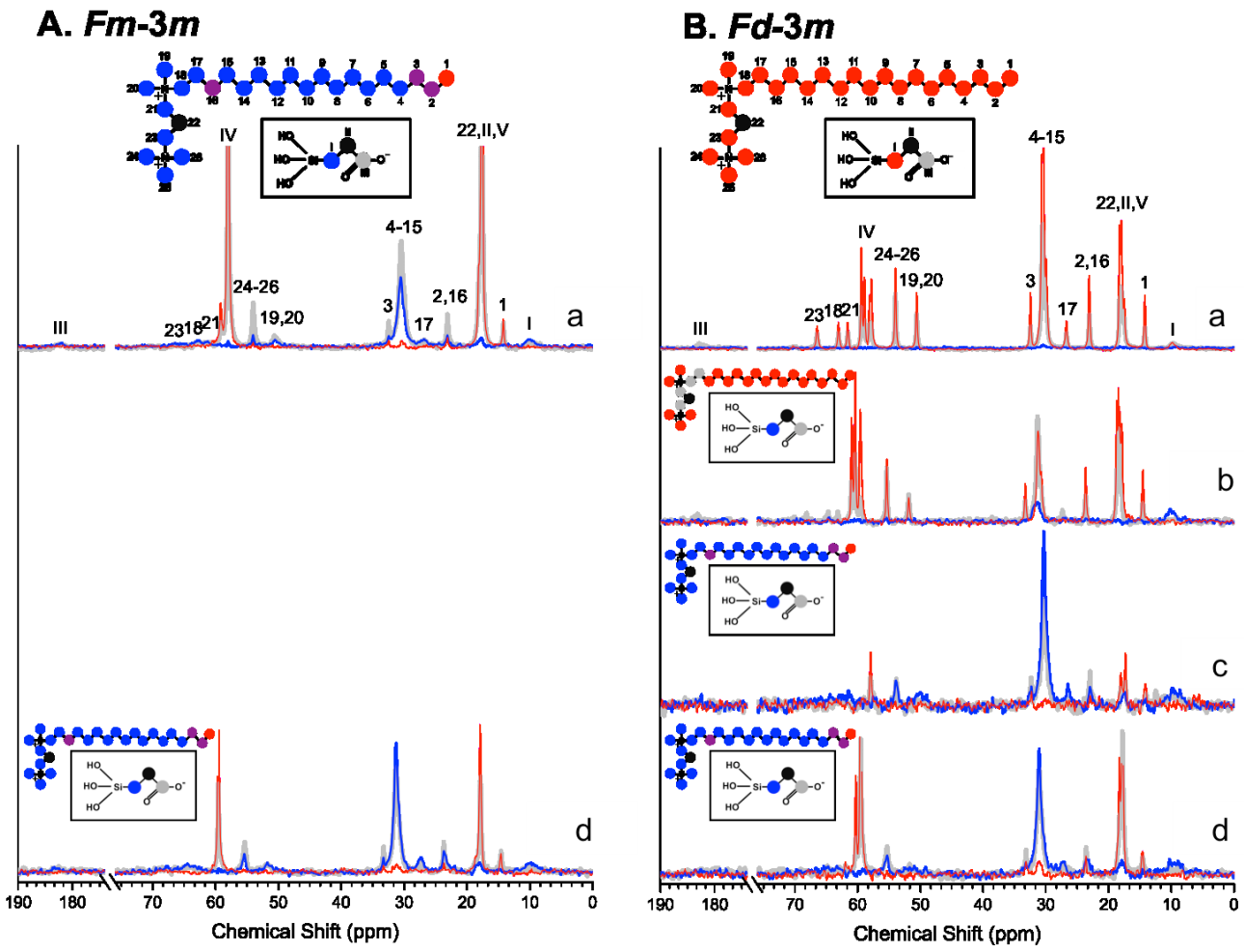

Figure 4. ^{13}C MAS NMR spectra (DP - grey, CP - blue, and INEPT - red) of A) *Fm*$\bar{3}$*m* and B) *Fd*$\bar{3}$*m*, at different stages of synthesis, a) after two hours of synthesis (before hydrothermal treatment), b) after 1.5 hours of hydrothermal treatment, c) after 7 hours of hydrothermal treatment, and d) after 2 days of hydrothermal treatment. The chemical molar composition of the reaction mixture was $C_{18\text{-}3\text{-}1}$: 2CSDA: xHCl: 15TEOS: 2000H_2O, A) x=1.4, B) x=1.8. The Arabic numbers refer to the surfactant molecule and the roman to the CSDA (I-III) and ethanol/TEOS (IV-V). The segments are coloured according to the signals. The intensities in the same set of DP-CP-INEPT experiments were normalized against the DP intensity of the $-CH_3$ group in the tail (1). All spectra are plotted at the same scale.

It is clear that the $Fd\bar{3}m$ and $Fm\bar{3}m$ structure give rise to very different CP and INEPT signals after 2 hours of synthesis; in the $Fd\bar{3}m$ structure, all segments have very high INEPT intensity, corresponding to mobile (isotropic) behavior. Virtually no CP signal was detected. The $Fm\bar{3}m$ structure, on the other hand, was dominated by CP signal, except a few segments in the chain. This indicates that the head group and the carbon chain are quite rigid and show anisotropic behavior. Hence, after 2 hours reaction, the $Fd\bar{3}m$ structure is still a soft and flexible system, while the $Fm\bar{3}m$ structure is already established. When the syntheses are completed, after 2 days of hydrothermal treatment, the resulting structures showed similar NMR spectra with high CP intensity for both the surfactant and the CSDA. This confirms that both structures are fixed. For the formation of $Fd\bar{3}m$ structure more information on the process is obtained; after 1.5 hours of hydrothermal treatment, the $-CH_2$ groups (17, 18, 21, 23) close to a nitrogen in the surfactant only show DP signal, which means that they are in very slow movement (correlation time between 0.1-10 μs) while the other segments still have high INEPT signal (correlation time < 0.1 μs). It indicates that, at this moment, the surfactant head group starts to become fixed and at the same time we observe that the CSDA is fixed. After 7 hours of hydrothermal treatment, where the spectra is equivalent to the one after 2 days, the surfactant segments are mostly rigid, except for the $-CH_3$ group in the tail (1) that continues to show isotropic reorientation in fast dynamical regime (correlation time < 1 ns). The 2, 3 and 16 $-CH_2$ segments have both INEPT and CP signals, indicating that they have a fast but anisotropic behavior. However, since the signal of segments 2 and 16 overlap, we cannot distinguish the exact behavior of these two segments. Possibly 2 is mobile while 16 is rigid. This behavior is the same for spectra in Figure 4, A-a, A-d, B-c and B-d.

We also performed SAXD measurements complementary to the ^{13}C PT ssNMR measurements (Support information Figure S7). 2 hours into the reaction the SAXD pattern of the $Fm\bar{3}m$ synthesis is dominated by peaks that correspond to this space group, having equivalent lattice spacing. However the $Fd\bar{3}m$ structure is not well developed at this time and a clear pattern is obtained after 1.5 h of hydrothermal treatment. The SAXD data are hence in agreement with the PT ssNMR. When the segments are rigid the structure is established. We can also see that when the surfactant head group moves slowly, while the chain is still mobile, the structure is established (at 1.5 hours of hydrothermal treatment). In addition the CSDA is rigid at this point.

The NMR combined with the SAXD results are in agreement with the findings presented above; the $Fm\bar{3}m$ structure, formed at a pH where the kinetics of the silica condensation is fast, contains surfactant and CSDA that quickly get stuck in the structure (low INEPT signal already after 2 h), whereas the $Fd\bar{3}m$ structure, which formation relies on slow condensation, contains surfactant and CSDA molecules that are still flexible after 2 hours of reaction.

According to Huo *et al*., [33] the $Fm\bar{3}m$ structure has, for this type of surfactant, only been found in mesoporous silica systems and not in the corresponding pure surfactant-water liquid-crystals. The formation of $Fm\bar{3}m$ structure seems to be a result of a process that arrives at a dynamical arrest; the spherical shape of the close-packed entities is conserved as a consequence of silica crosslinking, a process facilitated for instance when the hydrolysis step is removed. When, on the other hand, the surfactant-silica system has time to rearrange, the $Fd\bar{3}m$ structure, also found in the surfactant-water system, is the preferred structure.

4. Conclusion

In this work we show that the reaction kinetics of the silica source has a determining role in the structure formation; generally this is overlooked in mechanistic discussions.

Here we show that the pH dependence of the hydrolysis rate of TEOS is the origin of the structural change between $Fm\bar{3}m$ and $Fd\bar{3}m$, rather than the previously suggested ionization degree mechanism.[10, 13] We conclude that the $Fd\bar{3}m$ structure has a slower formation process than the $Fm\bar{3}m$ structure, which is in agreement with the description of "soft-cage" packing for the $Fd\bar{3}m$ structure.[11] Possibly formation of $Fm\bar{3}m$ relies on a system that arrives at a dynamical arrest induced by silica condensation.

In addition, both structures have similar extent of cross-linking of silica. However, formation of the $Fd\bar{3}m$ structure requires more CSDA, and, possibly, the cross-linking of CSDA is lower than that of the $Fm\bar{3}m$ structure.

Finally, we have shown that ^{13}C PT ssNMR experiments can provide valuable information on dynamical characteristics at an atomic level of surfactants and CSDA in mesoporous silica systems.

Acknowledgement

We are very grateful to Shunai Che at Shangai Jiao Tong University, P. R. China, for providing the surfactant and for sharing her extensive expertise in the CSDA synthesis route. We are also thankful to Julien Schmitt and Olle Söderman at Lund University, Sweden, Barbara Gore at University of Manchester, UK, and Lu Han at Shanghai Jiao Tong University, P. R. China, for experimental expertise and/or insightful discussions. R. L. and V. A. are grateful for

financial support from the Swedish Research Council via project grants and the Linneaus Centre of Excellence “Organizing Molecular Matter”.

Associated Content

Supporting Information

Figure S1, S4 and S7 show additional SAXD patterns. Figure S2 shows the ^{29}Si NMR spectrum of hydrolyzed TEOS and details the NMR measurements. Figure S3 shows Nitrogen adsorption-desorption isotherms and corresponding pore size distribution curves of the calcined samples shown in Figure 1. Figure S5 shows the solid-state ^{29}Si NMR spectra including the fitting. Figure S6 shows SAXD patterns and ^{13}C PT ssNMR spectra of liquid crystal of the pure $C_{18\text{-}3\text{-}1}$/water system including the measurements details.

This information can be found on the internet at http://pubs.acs.org.

Author Information

Corresponding Author:

* Email: viveka.alfredsson@fkem1.lu.se. Tel: +46-46-222 81 55. Fax: +46-46-222 44 13.

Notes

The authors declare no competing financial interest.

References

1. Soler-illia, G. J. D.; Sanchez, C.; Lebeau, B.; Patarin, J., Chemical Strategies to Design Textured Materials: From Microporous and Mesoporous Oxides to Nanonetworks and Hierarchical Structures. *Chem. Rev.* **2002**, *102*, 4093-4138.

2. Yanagisawa, T.; Shimizu, T.; Kuroda, K.; Kato, C., The Preparation of Alkyltrimethylammonium-Kanemite Complexes and Their Conversion to Microporous Materials. *Bull. Chem. Soc. Jpn.* **1990**, *63*, 988-992.

3. Kresge, C. T.; Leonowicz, M. E.; Roth, W. J.; Vartuli, J. C.; Beck, J. S., Ordered Mesoporous Molecular-Sieves Synthesized by a Liquid-Crystal Template Mechanism. *Nature* **1992**, *359*, 710-712.

4. Zhao, D. Y.; Feng, J. L.; Huo, Q. S.; Melosh, N.; Fredrickson, G. H.; Chmelka, B. F.; Stucky, G. D., Triblock Copolymer Syntheses of Mesoporous Silica with Periodic 50 to 300 Angstrom Pores. *Science* **1998**, *279*, 548-552.

5. Wan, Y.; Shi, Y.; Zhao, D., Designed Synthesis of Mesoporous Solids Via Nonionic-Surfactant-Templating Approach. *Chem. Commun.* **2007**, 897-926.

6. Che, S.; Garcia-Bennett, A. E.; Yokoi, T.; Sakamoto, K.; Kunieda, H.; Terasaki, O.; Tatsumi, T., A Novel Anionic Surfactant Templating Route for Synthesizing Mesoporous Silica with Unique Structure. *Nature Materials* **2003**, *2*, 801-805.

7. Gao, C.; Che, S., Organically Functionalized Mesoporous Silica by Co-Structure-Directing Route. *Adv. Funct. Mater.* **2010**, *20*, 2750-2768.

8. Che, S.; Liu, Z.; Ohsuna, T.; Sakamoto, K.; Terasaki, O.; Tatsumi, T., Synthesis and Characterization of Chiral Mesoporous Silica. *Nature* **2004**, *429*, 281-284.

9. Han, L.; Terasaki, O.; Che, S., Carboxylic Group Functionalized Ordered Mesoporous Silicas. *J. Mater. Chem.* **2011**, *21*, 11033-11039.

10. Han, L.; Sakamoto, Y.; Terasaki, O.; Li, Y.; Che, S., Synthesis of Carboxylic Group Functionalized Mesoporous Silicas (Cfmss) with Various Structures. *J. Mater. Chem.* **2007**, *17*, 1216-1221.

11. Sakamoto, Y.; Han, L.; Che, S.; Terasaki, O., Structural Analyses of Intergrowth and Stacking Fault in Cage-Type Mesoporous Crystals. *Chem. Mater.* **2009**, *21*, 223-229.

12. Han, L.; Sakamoto, Y.; Che, S.; Terasaki, O., Insight into the Defects of Cage-Type Silica Mesoporous Crystals with Fd$\bar{3}$M Symmetry: Tem Observations and a New Proposal of "Polyhedron Packing" for the Crystals. *Chem. Eur. J.* **2009**, *15*, 2818-2825.

13. Han, L. Synthesis and Characterization of Functionalized Silica Mesoporous Crystals. Stockholm University, Stockholm, Sweden, 2010.

14. Kjellman, T.; Alfredsson, V., The Use of in Situ and Ex Situ Techniques for the Study of the Formation Mechanism of Mesoporous Silica Formed with Non-Ionic Triblock Copolymers. *Chem. Soc. Rev.* **2013**, *42*, 3777-3791.

15. Kresge, C. T.; Roth, W. J., The Discovery of Mesoporous Molecular Sieves from the Twenty Year Perspective. *Chem. Soc. Rev.* **2013**, *42*, 3663-3670.

16. Han, L.; Che, S., Anionic Surfactant Templated Mesoporous Silicas (Amss). *Chem. Soc. Rev.* **2013**, *42*, 3740-3752.

17. Brinker, C. J., Hydrolysis and Condensation of Silicates - Effects on Structure. *J. Non-Cryst. Solids* **1988**, *100*, 31-50.

18. Kajihara, K., Recent Advances in Sol–Gel Synthesis of Monolithic Silica and Silica-Based Glasses. *J. Asian Ceram. Soc.* **2013**, 13.

19. Nowacka, A.; Mohr, P. C.; Norrman, J.; Martin, R. W.; Topgaard, D., Polarization Transfer Solid-State Nmr for Studying Surfactant Phase Behavior. *Langmuir* **2010**, *26*, 16848-16856.

20. Nowacka, A.; Bongartz, N. A.; Ollila, O. H. S.; Nylander, T.; Topgaard, D., Signal Intensities in H-1-C-13 Cp and Inept Mas Nmr of Liquid Crystals. *J. Magn. Reson.* **2013**, *230*, 165-175.

21. Pines, A.; Waugh, J. S.; Gibby, M. G., Proton-Enhanced Nuclear Induction Spectroscopy - Method for High-Resolution Nmr of Dilute Spins in Solids. *J. Chem. Phys.* **1972**, *56*, 1776-&.

22. Morris, G. A.; Freeman, R., Enhancement of Nuclear Magnetic-Resonance Signals by Polarization Transfer. *J. Am. Chem. Soc.* **1979**, *101*, 760-762.

23. Alonso, B.; Massiot, D., Mufti-Scale Nmr Characterisation of Mesostructured Materials Using H-1 -> C-13 through-Bond Polarisation Transfer, Fast Mas, and H-1 Spin Diffusion. *J. Magn. Reson.* **2003**, *163*, 347-352.

24. Elena, B.; Lesage, A.; Steuernagel, S.; Bockmann, A.; Emsley, L., Proton to Carbon-13 Inept in Solid-State Nmr Spectroscopy. *J. Am. Chem. Soc.* **2005**, *127*, 17296-17302.

25. Warschawski, D. E.; Devaux, P. F., H-1-C-13 Polarization Transfer in Membranes: A Tool for Probing Lipid Dynamics and the Effect of Cholesterol. *J. Magn. Reson.* **2005**, *177*, 166-171.

26. Nowacka, A.; Douezan, S.; Wadso, L.; Topgaard, D.; Sparr, E., Small Polar Molecules Like Glycerol and Urea Can Preserve the Fluidity of Lipid Bilayers under Dry Conditions. *Soft Matter* **2012**, *8*, 1482-1491.

27. Bennett, A. E.; Rienstra, C. M.; Auger, M.; Lakshmi, K. V.; Griffin, R. G., Heteronuclear Decoupling in Rotating Solids. *J. Chem. Phys.* **1995**, *103*, 6951-6958.

28. Boissiere, C.; Larbot, A.; Bourgaux, C.; Prouzet, E.; Bunton, C. A., A Study of the Assembly Mechanism of the Mesoporous Msu-X Silica Two-Step Synthesis. *Chem. Mater.* **2001**, *13*, 3580-3586.

29. Sugahara, Y.; Inoue, T.; Kuroda, K., Si-29 Nmr Study on Co-Hydrolysis Processes in Si(Oet)(4)-Rsi(Oet)(3)-Etoh-Water-Hcl Systems (R=Me,Ph): Effect of R Groups. *J. Mater. Chem.* **1997**, *7*, 53-59.

30. Steel, A.; Carr, S. W.; Anderson, M. W., Si-29 Solid-State Nmr-Study of Mesoporous M41s Materials. *Chem. Mater.* **1995**, *7*, 1829-1832.

31. Sayari, A.; Hamoudi, S.; Yang, Y.; Moudrakovski, I. L.; Ripmeester, J. R., New Insights into the Synthesis, Morphology, and Growth of Periodic Mesoporous Organosilicas. *Chem. Mater.* **2000**, *12*, 3857-3863.

32. Hagslatt, H.; Soderman, O.; Jonsson, B., Divalent Surfactants - Experimental Results and Theoretical Modeling of Surfactant Water Phase-Equilibria. *Langmuir* **1994**, *10*, 2177-2187.

33. Huo, Q. S.; Leon, R.; Petroff, P. M.; Stucky, G. D., Mesostructure Design with Gemini Surfactants - Supercage Formation in a 3-Dimensional Hexagonal Array. *Science* **1995**, *268*, 1324-1327.

TOC

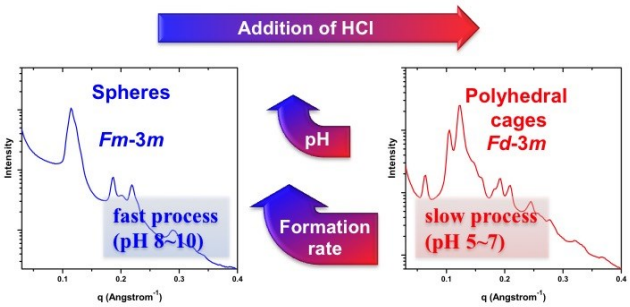
Addition of HCl
Spheres
Fm-3m
fast process
(pH 8~10)
pH
Formation
rate
Polyhedral
cages
Fd-3m
slow process
(pH 5~7)
Intensity
q (Angstrom-1)